frontiers in Energy Research

ORIGINAL RESEARCH
published: 28 June 2021
doi: 10.3389/fenrg.2021.703676

Holey Graphene–Enabled Solvent-Free Preparation of Ultrahigh Mass Loading Selenium Cathodes for High Areal Capacity Lithium–Selenium Batteries

Christian O. Plaza-Rivera[1], Rocco P. Viggiano[2], Donald A. Dornbusch[2], James J. Wu[3], John W. Connell[4] and Yi Lin[5]**

[1]NASA Interns, Fellows, and Scholars (NIFS) Program, NASA Langley Research Center, Hampton, VA, United States, [2]Materials Chemistry and Physics Branch, NASA Glenn Research Center, Cleveland, OH, United States, [3]Photovoltaic and Electrochemical Systems Branch, NASA Glenn Research Center, Cleveland, OH, United States, [4]Advanced Materials and Processing Branch, NASA Langley Research Center, Hampton, VA, United States, [5]National Institute of Aerospace, Hampton, VA, United States

OPEN ACCESS

Edited by:
Matthew Li,
Argonne National Laboratory (DOE), United States

Reviewed by:
Xingxing Gu,
Chongqing Technology and Business University, China
Xiaolei Wang,
University of Alberta, Canada

***Correspondence:**
John W. Connell
john.w.connell@nasa.gov
Yi Lin
yi.lin-1@nasa.gov

Specialty section:
This article was submitted to Electrochemical Energy Conversion and Storage, a section of the journal Frontiers in Energy Research

Received: *30 April 2021*
Accepted: *31 May 2021*
Published: *28 June 2021*

Citation:
Plaza-Rivera CO, Viggiano RP, Dornbusch DA, Wu JJ, Connell JW and Lin Y (2021) Holey Graphene–Enabled Solvent-Free Preparation of Ultrahigh Mass Loading Selenium Cathodes for High Areal Capacity Lithium–Selenium Batteries. Front. Energy Res. 9:703676. doi: 10.3389/fenrg.2021.703676

Solvents and binders are typical requirements in conventional lithium ion battery electrode fabrication to enable intimate material mixing, mechanical robustness, and reproducibility. However, for high energy density conversion chemistry cathodes such as sulfur (S) and selenium (Se), the time-consuming solvent-based methods are proven unreliable to achieve high mass loading cathodes with sufficient quality. Here, we report a facile solvent-free and binder-free method to prepare high mass loading composite Se cathodes that is enabled by the use of holey graphene (hG) as a lightweight conductive scaffold. Holey graphene is a derivative of graphene and can be dry-pressed into robust discs by itself. It can also serve as a matrix to host materials such as Se for composite disc preparation in a mix-and-press process free of solvent and binder. The method allows the preparation of ultrahigh Se content cathodes (up to 90 wt% Se) and ultrahigh Se mass loading (up to 15.6 mg cm^{-2} in this work). These cathodes exhibit excellent Se utilization, high areal capacity (up to 9 mAh cm^{-2}), and good rate performance. The dry-press approach also allows for the preparation of a layered composite cathode architecture, where a thin hG layer is inserted between the composite and the current collector to improve the electrical contact. A solvent-free approach is also used to prepare hG-based hybrids with metal sulfides to be incorporated into a composite cathode to help entrap soluble polyselenide intermediates. The hybrid material is compatible with the solvent-free mix-and-press electrode fabrication approach and shows promise in improving the Se retention. While further improvements are still required, this work demonstrates the outstanding potential of using this facile, solvent-free approach enabled by hG for fabrication of high-performance, high mass loading conversion chemistry cathodes.

Keywords: lithium–selenium batteries, holey graphene, high mass loading electrodes, high areal capacity electrode, electrode architecture

INTRODUCTION

The need for higher energy density batteries in demanding applications such as electric vehicles and aircrafts has stimulated research in conversion-type battery chemistries such as lithium–sulfur (Li-S) and lithium–selenium (Li-Se) pairs (Eftekhari, 2017; Kumar et al., 2018; Gu and Lai, 2019; Gu et al., 2019; Bhargav et al., 2020; Huang et al., 2020; Zhao, et al., 2020; Sun, et al., 2021). The two types of batteries share very similar reaction mechanisms during discharge and charge cycling, in which they both go through intermediates that are soluble in traditional liquid electrolytes. Selenium has lower theoretical specific energy than S (675 vs. 1,672 mAh g^{-1}), but is much more electrically conductive (10^{-5} vs. 10^{-30} S/cm). In these batteries, higher current often results in lower material utilization, thus resulting in lower available energy. Because of the higher conductivity, Se-based cathodes may even outperform S cathodes in energy at sufficiently high current densities. Due to their chemical similarity, it has also been proposed that a hybrid compound of these two elements may provide active conversion-type materials with more balanced energy and power performance (Abouimrane et al., 2012; Xu, et al., 2017). In this context, dedicated studies on Li-Se batteries, although comparably much less than those on Li-S batteries, would be helpful in providing more insight into the Li/S-Se battery chemistry and their potential toward a balanced energy and power performance. For Li-Se batteries, significant challenges remain in almost all aspects of the electrochemical cell system, including cathode design and fabrication, Li metal anode stability and utilization, electrolyte selection, approaches to attenuate polyselenide shuttling, and strategies to improve overall energy density by, for example, increasing Se loading and reducing the electrolyte-to-Se ratio (Eftekhari, 2017; Gu and Lai, 2019; Gu et al., 2019; Sun et al., 2021).

Battery electrodes typically consist of the requisite active material, conductive additives to improve electrical conductivity, and polymer binders to keep the electrode integral. Polymer binders added to the electrode mixture do not directly contribute to battery energy storage; instead, it may experience parasitic reactions. Thus, its content should always be minimized in the formulation. During the conventional multistep fabrication process, these materials are mixed in a solvent to form a slurry, which is then coated on a current collector and allowed to dry to form an electrode sheet. To ensure homogenous mixing and slow solvent evaporation for high-quality electrodes, high boiling point organic solvents, usually toxic, are often used. High-quality Li ion battery electrodes have been fabricated using the above conventional approach in research laboratories and commercially (Wenzel et al., 2015; Kraytsberg and Ein-Eli, 2016; Hawley and Li, 2019).

Most Li ion battery electrodes undergo an intercalation process, where only Li ions move in and out of the electrode structure (Manthiram, 2020). Most of these electrodes experience little volume change during charge and discharge. In comparison, the conversion-type electrodes such as Se experience much more severe volume changes because of the significant density difference of the electrode active material in the charge state (Se: 4.8 g cm^{-3}) vs. discharge state (Li_2Se: 2 g cm^{-3}). While the final discharge product, that is, Li_2Se, is a solid, the reaction intermediates generated around a third of discharge are in a polymeric form, that is, polyselenides, which are soluble in common liquid electrolytes. These drastic physical changes of the active material during the battery reaction, especially at a practical mass loading level (~5 mg cm^{-2} and above), make it extremely challenging to fabricate electrodes with acceptable performance. Conventional slurry-based electrode fabrication methods are mostly optimized for intercalation-type electrodes. When applied to conversion-type active materials, it often yields inferior coating quality with crack formation as the mass loading is increased, not to mention the poor performance during cycling that is likely related to the severe physical stress caused by the volume change of the cathode material (Pope and Aksay, 2015; Chung et al., 2018; Huang et al., 2020).

Recently, our group discovered that holey graphene (hG), a derivative of graphene, can be compressed from its dry powder form into robust solid architectures of various shapes either by itself or as a host for other materials (Han et al., 2017; Lin et al., 2019). The dry compressibility is uniquely attributed to the nanometer-sized holes through the nanosheet surface, which originate from the intrinsic defects of the parent graphene, and therefore do not significantly affect the typical characteristics of graphene as an electrode material. With high electrical conductivity, high surface area, and mechanical robustness, hG has been shown to be an excellent and versatile scaffold material applicable for various forms of energy storage. The dry-pressed neat hG electrodes were directly used for energy storage devices such as supercapacitors (Walsh et al., 2016) and air cathodes for lithium–oxygen (Li-O_2) batteries (Lin et al., 2017). It can also serve as an effective host for dry-pressed composite electrodes with active materials from both intercalation [e.g., lithium iron phosphate (LFP) (Kirsch et al., 2019) and lithium nickel cobalt manganese (NCM) (Walker et al., 2020)] and conversion (e.g., S) chemistries (Lin et al., 2019). The dry-press electrode fabrication procedure is facile and does not require the use of any solvent or binder. All the resultant electrodes exhibited excellent performance with high active material utilization due to the effectiveness of the conductive hG scaffold. With the unique dry compression electrode fabrication approach, the use of hG is particularly beneficial for high-quality, high mass loading electrodes that are required in practical applications.

Here, we demonstrate the use of hG as an effective host for the dry-press fabrication of high mass loading Se cathodes with the Se content up to 90%. The dry-press approach also allows the fabrication of a neat hG layer between the cathode and the current collector to reduce the contact resistance. We further demonstrate that molybdenum disulfide (MoS_2), a transition metal sulfide that may help retain soluble polyselenides, can be grown onto hG in a solvent-free approach. The MoS_2@hG hybrid is shown to be compatible with the dry-press approach for Se cathodes with improved cycling performance.

EXPERIMENTAL SECTION

Materials

Holey graphene (hG) was prepared from graphene (Vorbeck Materials) using the established one-step air oxidation procedure previously reported (Lin et al., 2015). Bis(trifluoro-methane) sulfonimide lithium salt (LiTFSI; 99.95%), lithium nitrate ($LiNO_3$; 99.99%), 1,2-dimethoxyethane (DME; anhydrous, 99.5%), 1,3-dioxolane (DOL; anhydrous, 99.8%), selenium (Se; powder, ~100 mesh, 99.99%), and ammonium tetrathiomolybdate [$(NH_4)_2MoS_4$; 99.97%] were purchased from Sigma-Aldrich. Lithium chips (15.6 mm diameter, 0.45 mm thickness), Celgard membrane (0.025 mm thickness), and aluminum (Al) foil (0.015 mm thickness) were purchased from MTI Corporation. All chemicals for battery assembly were handled inside an Ar-filled glove box with O_2 and H_2O concentrations < 1 ppm. The solvents were dried over freshly regenerated molecular sieves before using them for electrolyte preparation. All other materials and chemicals were used as received.

MoS_2@hG Hybrid

In a typical experiment, $(NH_4)_2MoS_4$ (0.85 mmol; ~220 mg) powder was mixed with hG powder (8.5 mmol; ~100 mg) *via* a ball mill (SPEX CertiPrep 8000D High-Energy Shaker Mill) for 30 s. The resultant solid mixture was heated up in a N_2 atmosphere from room temperature to 400°C in 1 h (ramp rate ~6.3°C min^{-1}) and held for 3 h. After cooling to room temperature, the MoS_2@hG hybrid product was obtained.

hG/Se Composite Mixture and Cathodes

Desirable amounts of hG powder and Se powder were added into a 20-ml zirconia vial (SPEX CertiPrep) with two zirconia balls (SPEX CertiPrep, d = 1.3 cm). The powders were milled for just 10 s on a high-energy ball mill (SPEX CertiPrep 8000D) to yield the hG/Se composite mixture. For cathode disc preparation, a desirable amount of the composite mixture was placed into a stainless steel pressing die (MTI Corporation; Model EQ-Die-15D; the manufacturer identified the inner diameter as 14.85 mm). Two pieces of precisely cut (15 mm in diameter) Al foil discs were used as separation layers to prevent unwanted material adhesion to the top and bottom inner die surfaces. The composite mixture was then pressed at 200 MPa (Carver Hydraulic Unit Model #3925) and held for ~10 min, generating a 1.73 cm^2 cathode disc (after peeling of both Al foil discs), which was denoted as hG/Se-*x*%, with *x*% being the weight percentage of Se in the mixture.

For each layered composite cathode disc with a thin layer of neat hG (hG|hG/Se-*x*%, where "hG|" is used to denote the added interlayer), a desirable amount of hG powder (typically 2.9 mg cm^{-2}) was added to the die before or after the composite powder. The entire powdery ensemble was then pressed together in a single step to form the final disc.

For the cathode discs with MoS_2@hG, the MoS_2@hG powder was first mixed with neat hG powder in a weight ratio of 1:1 using the ball mill for 10 s to form a mixture (MoS_2-hG). The ball-milling time was intentionally kept brief to prevent unwanted self-condensation of hG sheets while still rendering adequate overall powder mixing. This mixture was then used as the compressible host for Se for subsequent mix-and-press process to form electrodes with MoS_2-hG/Se-*x*% or hG|MoS_2-hG/Se-*x*% configurations.

Li-Se Battery Coin Cells

Li-Se batteries were assembled using typical CR2032 coin cell parts (MTI Corporation) with a hydraulic crimper (MTI Corporation, Model MSK-110) inside an Ar-filled glove box (MBraun Labmaster 130), with O_2 and H_2O concentrations < 1 ppm. One of the various hG/Se composite discs and a piece of the Li chip were used as the cathode and the anode, respectively, with a 19-mm diameter Celgard membrane as the separator. The electrolytes were 1 M LiTFSI and 0.2 M $LiNO_3$ in DME:DOL (1:1, v/v). The E/Se ratio (ml/g) used throughout this work was kept at approximately 6.5.

Measurements

Scanning and transmission electron microscopy (SEM and TEM) images were acquired using a Hitachi S-5200 field emission SEM (FE-SEM) system. Lower magnification SEM images were also acquired on a TESCAN VEGA3 tungsten thermionic emission SEM system, both operated at an acceleration voltage of 20 kV. The Hitachi S-5200 SEM is equipped with a Thermo Scientific UltraDry energy dispersive spectroscopy (EDS) detector, while the TESCAN system is also equipped with an EDAX Octane Elect EDS system. A Rigaku SmartLab X-ray Diffractometer with a Cu Kα radiation source was employed for XRD analyses. Surface DC conductivity was measured with a four-point probe system (Signatone, QuadPro Resistivity Wafer Mapping System) at room temperature. Conductivity values of each sample were calculated and averaged with resistivity measured at five different locations. Battery discharge/charge measurements were conducted on a BST8-MA or a BST8-300-CST 8-Channel Battery Analyzer (MTI Corp.). Areal current densities (J_A) used were calculated according to the area of cathode (1.73 cm^2) and ranged from 0.5 to 5 mA/cm^2 in this work. Electrochemical impedance spectroscopy (EIS) and cyclic voltammetry (CV) were conducted on a BioLogic VMP-3 electrochemical station. EIS was measured at the open circuit potential in the frequency range of 1 MHz to 0.01 Hz, with an amplitude of 10 mV and 10 points measured per decade. CV was scanned in the voltage range of 1.4–2.8 V at a scan rate of 0.05 mV s^{-1}.

RESULTS AND DISCUSSION

By taking advantage of the unique property of hG as a dry compressible matrix, ultrahigh mass loading hG/Se cathodes were conveniently fabricated without any solvents or binders in a facile two-step mix-and-press process (**Figure 1**). This mix-and-press technique enabled by hG allows for extremely facile preparation of composite disc cathodes with precise and tunable active material loadings. With practical loading in mind, this work focuses on cathodes with Se contents (Se%) ≥ 50 wt% and areal Se mass loadings (m_{Se}) ≥ 8.7 mg/cm^2.

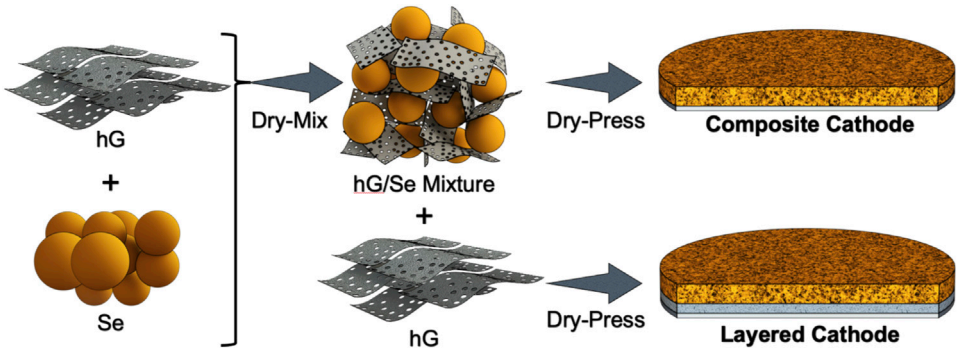

FIGURE 1 | Schematic illustration of the solvent-free mix-and-press process: **(left)** mix hG and Se powder into the hG/Se composite mixture; **(right top)** directly press the hG/Se composite mixture onto the current collector to form a composite cathode disc; **(right bottom)** press sequentially loaded hG powder and the composite mixture powder to form a layered cathode disc, with a hG layer between the composite and the current collector.

The as-prepared hG/Se cathode discs were dense and conductive, with encapsulated Se retaining their physical properties. Higher Se contents led to an increase of disc density and a decrease in conductivity, both in a nonlinear fashion (**Figure 2A**). For example, a hG/Se disc with 50% Se (hG/Se-50%) exhibited a density of 1.4 g cm^{-3}, with surface conductivity as high as 563 S cm^{-1}. At 90% Se (hG/Se-90%), the disc density increased to 2.5 g cm^{-3} while still retaining a high surface conductivity of 163 S cm^{-1}. In comparison, a hG/S-90% disc using the same fabrication method exhibited a density of 1.8 g cm^{-3} and a surface conductivity of 10 S cm^{-1} (Lin et al., 2019), which is consistent with the lower density (density: 2.1 g cm^{-3}) and much lower electrical conductivity (on the order of 10^{-30} S cm^{-1}) of S than Se.

XRD patterns of the composite discs (**Figure 2B**) matched well with that of the neat Se powder and the JCPDS database (PDF# 06-0362). The broad feature at ~ 26° is attributed to the (002) peak of graphitic carbon from the hG matrix. The internal morphology of the hG/Se composite discs was further visualized and analyzed using cross-sectional SEM and elemental mapping with EDS. A low-magnification SEM image (**Figure 2C**) shows the long-range, even thickness across the hG/Se composite disc. At a higher magnification with the corresponding C-map (**Figure 2D** and **Supplementary Figure S1**), the hG sheets can be seen to be horizontally aligned normal to the pressing direction. Micrometer-sized Se particles, with the same morphology as those in the neat powder (Plaza-Rivera et al., 2020), were well distributed throughout the cross section in between the hG sheets from the SEM image and the Se map (**Figure 2D**), suggesting excellent electrical contacts between the active material particles and the conductive scaffold. These observations strongly suggest that the mix-and-press process, despite its short duration in each step, was exceptionally effective. The process provided an intimate and uniform mixture of the active material Se with the conductive scaffold hG without altering the properties of either material at all these ratios investigated in this study.

The high mass loading hG/Se cathodes were assembled into coin cells each with a Li chip as the anode for electrochemical evaluations. In Li-Se battery chemistry, Se is converted into soluble polyselenides of various chain lengths in Li-Se batteries, similar to Li-S battery chemistry (Eftekhari, 2017). This is supported by the cyclic voltammetry (CV) data (**Figure 3A**, hG/Se-50% as an example), which show two reduction peaks at 2.10 and 1.86 V corresponding to long- and short-chain polyselenides, respectively. When reversing the current, the oxidation peak at 2.32 V with a shoulder at 2.37 V can be readily attributed to the completion of the Se regeneration cycle. At a high mass loading of 8.7 mg cm^{-2}, both reduction and oxidation peaks remained well defined, suggesting fast electrochemical kinetics, which is an indication of the effectiveness of the conductive hG scaffold.

Galvanostatic charge–discharge curves of the Li-Se battery cells at various current densities are shown in **Figure 3B**. The voltage behavior is in close agreement with the CV data (**Figure 3A**). For example, at an areal current density (J_A) of 0.5 mA cm^{-2}, there are two voltage plateaus at ~ 2.16 and ~2 V during discharge, corresponding to long- and short-chain polyselenides, respectively. The dual discharge voltage plateaus were also observed at higher current densities. At the same J_A, the charge reaction exhibited a single plateau at ~2.2 V, suggesting that the intermediate steps in the reverse battery reaction were much less distinct, commonly observed in the charge reactions of Li-S and Li-Se batteries in general (Eftekhari, 2017; Lin et al., 2019; Plaza-Rivera et al., 2020).

The initial discharge capacity for the battery cell with a hG/Se-50% cathode was as high as ~ 820 mAh g_{Se}^{-1} (7.1 mAh cm^{-2}) at 0.5 mA cm^{-2}. This value is even higher than the theoretical capacity of Se (675 mAh g_{Se}^{-1}), which is not unusual especially when the initial Se utilization is nearly complete. For example, a similar phenomenon was previously observed (Sun et al., 2021), where the excess capacity could be related to the partial decomposition of the electrolyte and the formation of the solid electrolyte interphase (SEI).

Notably, with a stepwise test protocol, where the battery cell was cycled 4 times each at J_A of 0.5, 1, 2, and 5 mA cm^{-2}, the capacity transitions between the adjacent J_A steps were not drastically evident (e.g., 410 mAh g_{Se}^{-1}at cycle 8 at 1 mA cm^{-2}

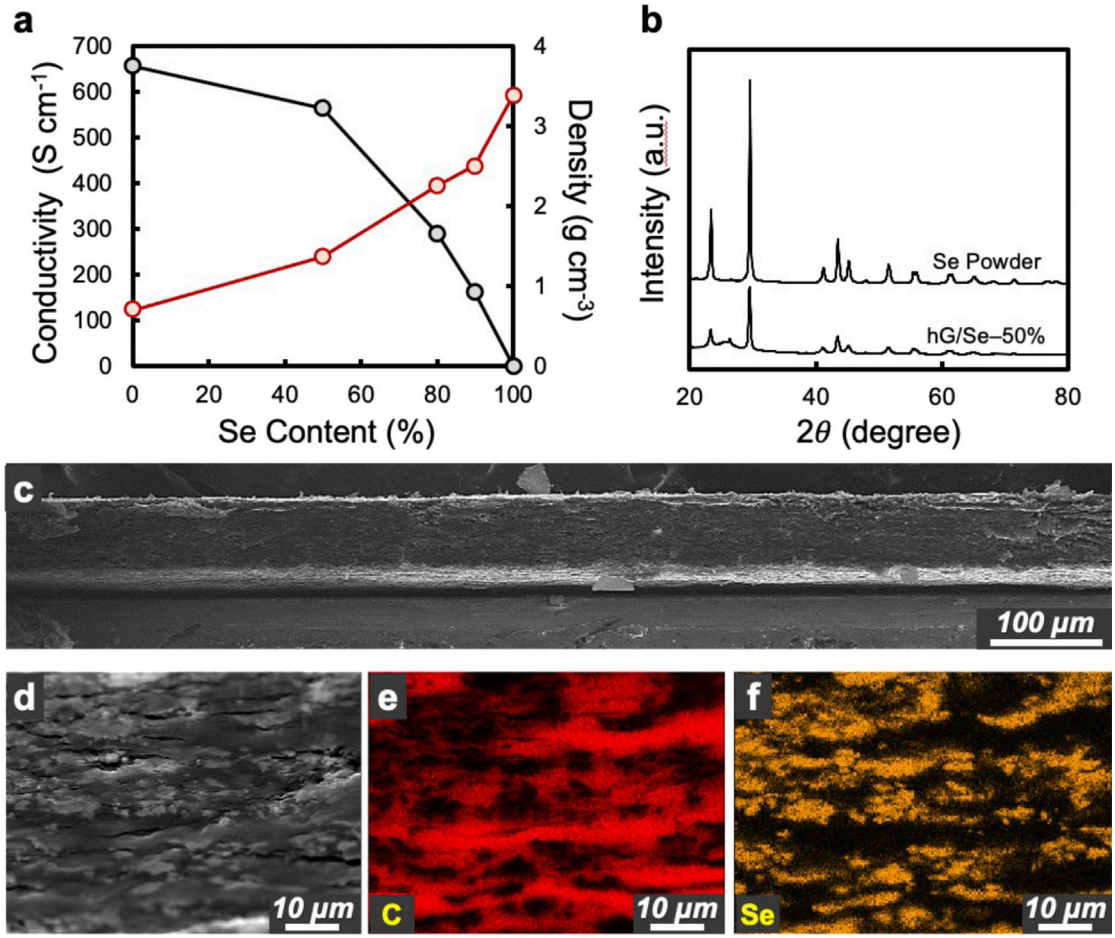

FIGURE 2 | Characterizations of hG/Se cathode discs: **(A)** dependence of surface conductivity (black color; left axis) and apparent density (red color; right axis) on the Se content (%) of various hG/Se discs; **(B)** XRD patterns of hG/Se-50% discs in comparison to the neat Se powder; **(C)** the low magnification SEM image of a cross-sectional view of hG/Se-50% discs; **(D)** a higher magnification view of the same disc and the corresponding EDS maps of C and Se elements.

vs. 396 mAh g_{Se}^{-1}at cycle 9 at 2 mA cm^{-2}) (**Figure 3C**; different J_A are color-coded). This is in stark contrast to the Li-S batteries with hG/S cathodes prepared under similar conditions, where there were distinct capacity drops where J_A was increased to the next step (Lin et al., 2019). This observation implies that the change in J_A did not result in any significant effect on the kinetics of the battery reaction. Therefore, these hG/Se cathodes are of much higher rate performance than similarly prepared hG/S cathodes, consistent with the fact that Se is a much more conductive active material than S (Eftekhari, 2017).

As mentioned previously, the mix-and-press approach for hG/Se cathode fabrication allowed the convenient increase of the Se content in the cathode simply by applying a higher Se:hG ratio during mixing. As an example, a hG/Se-90% disc (Se:hG = 9:1) was also prepared and assembled into Li-Se battery cells. With the total cathode loading remaining the same (hG + Se totaled 17.3 mg cm^{-2}), the Se mass loading improved from 8.7 mg cm^{-2} to 15.6 mg cm^{-2}. As shown in **Figure 3C**, the cell with an ultrahigh Se mass loading exhibited somewhat less but still high Se utilization, with the first discharge capacity around 574 mAh g_{Se}^{-1} (~85% utilization). With a higher Se mass loading, the areal capacity was much improved, despite the lower gravimetric capacity (**Figure 3D**). For example, at the fourth cycle (J_A = 0.5 mA cm^{-2}), the areal capacity improved from 4.1 (hG/Se-50%) to 5.6 mAh cm^{-2} (hG/Se-90%), a 36% improvement. In addition, even at such an ultrahigh Se content, there was still a lack of clear capacity transition during abrupt J_A changes in between the adjacent cycle steps, suggesting the battery reactions remained insensitive and kinetically viable at these J_A values. These high initial areal capacity values of these hG/Se cathodes, along with the ultrahigh Se mass loadings, are among the highest reported in the current literature (**Supplementary Table S1**).

The moderate adhesion of the Al current collector and the composite hG/Se cathode, especially at ultrahigh Se contents, resulted in higher interfacial resistance, as reflected in the broad CV peaks (**Figure 4A**) and high impedance revealed by EIS (**Figure 4B**). We observed that neat hG exhibited better

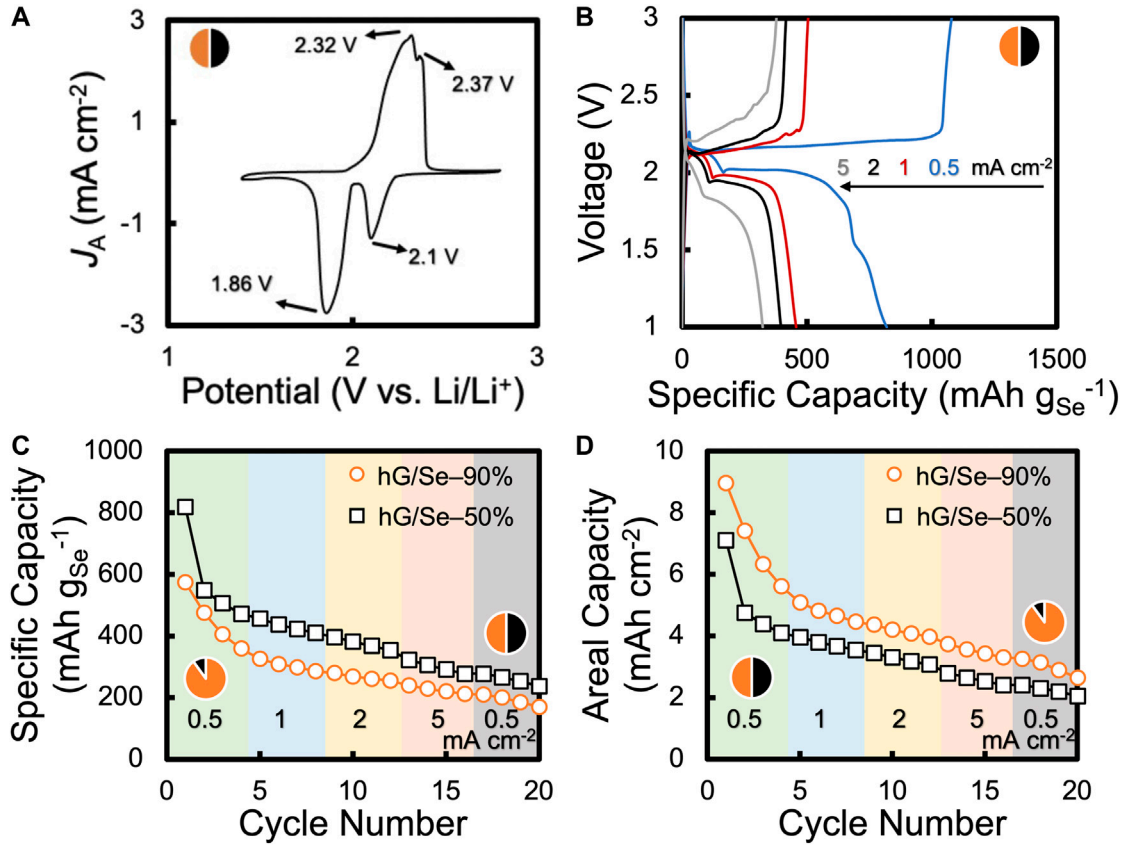

FIGURE 3 | Electrochemical performance of Li-Se battery cells with hG/Se cathodes: **(A)** CV of a cell with a hG/Se-50% cathode at 0.05 mV s^{-1}; **(B)** discharge and charge curves of a cell sequentially cycled at 0.5, 1, 2, and 5 mA cm^{-2} (each for 4 cycles); curves shown are the first cycle of each J_A segment, and comparisons of cells with a hG/Se-50% cathode and a hG/Se-90% cathode in terms of **(C)** specific capacity and **(D)** areal capacity.

adhesion to the Al surface than the composite hG/Se cathode. In order to improve the electrical interface, a thin neat hG layer was inserted between the Al current collector and the main composite layer. Such layered composite electrodes were conveniently fabricated by simply placing the desirable amount of hG powder before (or after) adding the composite powder into the pressing die. The compression was still completed in a single step (**Figure 1**). As shown in the SEM/EDS images in **Figure 4C**, the Se elements are confined in the composite layer, while hG sheets are distributed throughout the composite layer in addition to the neat layer. With a thin hG layer (2.9 mg cm^{-2}) adding to a hG/Se-90% cathode, the CV peaks of the resultant layered cathode (denoted as hG|hG/Se-90%; overall Se% = 77%) became much better defined (**Figure 4A**). In addition, the Nyquist plot from EIS measurement showed that both the bulk resistance (R_b, the intercept of *x*-axis) and the charge transfer resistance (R_{cf}, the size of semicircle) were much reduced (**Figure 4B**). Therefore, the lightweight, neat hG layer may thus be considered as a concept of an effective three-dimensional current collector that improved the electrical interface to the cathode composite (Lin et al., 2019).

Interestingly, the improvement of the electrical interface at the cathode current collector did not have a significant effect on the initial capacity, with the first discharge areal capacities at 9.0 and 8.7 mAh cm^{-2} for the hG/Se-90% and the hG|hG/Se-90% electrodes (both Se mass loadings = 15.6 mg cm^{-2}), respectively. This may be due to the rather rate-insensitive nature of the moderately conductive Se active material. Over cycling, however, the electrode with the additional hG layer did exhibit higher capacity (e.g., 1.7 vs. 1.2 mAh cm^{-2} at cycle 40) (**Figure 4D**). Unfortunately, all Li-Se battery cells with the hG/Se electrodes, with or without the additional hG interlayer, suffered extensive capacity loss over cycling due to the shuttling of polyselenide intermediates toward the Li metal anode as a result of their solubility and high mobility. The observed slight difference in the initial Coulombic efficiency shown in the inset of **Figure 4D** is rather insignificant considering the massive shuttling effect with or without the added hG layer. The detrimental shuttling effect was further amplified by the ultrahigh Se mass loading in these cells. Compared to Li-S batteries with similarly prepared hG/S cathodes (Lin et al., 2019), the observed capacity loss for Li-Se batteries was much more severe with much lower

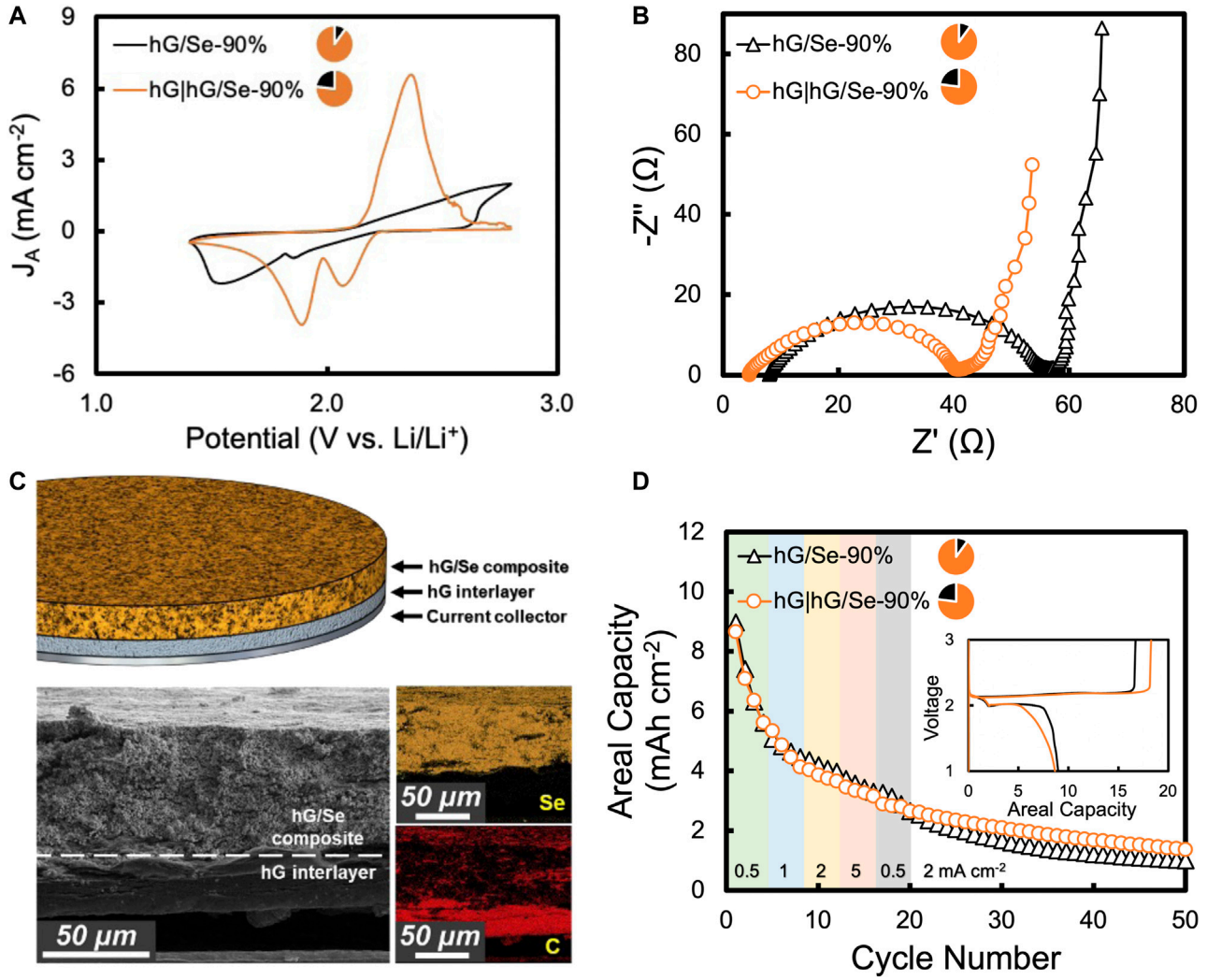

FIGURE 4 | hG/Se cathodes with a layered architecture, where a hG layer is inserted between the composite electrode and the current collector: **(A)** CV curve comparison and **(B)** Nyquist plot comparison from EIS measurements for battery cells with a hG/Se-90% cathode and a hG|hG/Se-90% cathode; **(C)** a schematic illustration of the layered electrode architecture and a SEM image with the corresponding Se and C maps from EDS; **(D)** cycling performance comparison of the two cells; inset shows the discharge–charge curves of the first cycle. Batteries were sequentially cycled at 0.5, 1, 2, and 5 mA cm^{-2}, each for 4 cycles, then at 2 mA cm^{-2}. In **(A, B, D)**, curves for the hG/Se-90% electrode and the hG|hG/Se-90% are black and orange colored, respectively.

percentages of capacity retention. Similar capacity loss was also previously observed for ultrahigh Se mass loading electrodes with a layered architectural configuration (Plaza-Rivera et al., 2020). Nevertheless, data of subsequent cycles 51–100 from the same cells of **Figure 4D** are shown in **Supplementary Figure S2**.

The extensive capacity loss over cycling prompted us to evaluate means of incorporating materials within the cathode that may entrap the soluble polyselenides to reduce their shuttling effect. Many transition metal oxides and sulfides, such as MnO_2, MoS_2, and TiO_2, have been shown in the literature to be useful for this purpose (Liu et al., 2017a; Rana et al., 2020; Ye and Lee, 2020; Sun et al., 2021). In order to be compatible with our unique solvent-free mix-and-press electrode fabrication approach, a MoS_2@hG hybrid was prepared using a convenient method previously developed in our laboratory that is also solvent free (Lin, et al., 2009). In this approach, $(NH_4)_2MoS_4$, a precursor for MoS_2, was mixed with hG powder at a desirable ratio (1:10 mol/mol in this work) *via* brief ball milling. The mixture was then heated to 400°C to allow thermal decomposition of $(NH_4)_2MoS_4$ into MoS_2 nanoparticles, which were well distributed and decorated on the hG surface (**Figure 5A**). The formation of MoS_2 nanoparticles was confirmed *via* XRD (**Supplementary Figure S3**), where peaks at 14.3, 33.5, 39.4, 49.4, and 58.2° correspond to MoS_2 (002), (100), (103), (105), and (110) phases, respectively (PDF# 37-1492). The broad peaks in XRD suggest ultrafine grain sizes for these nanoparticles. Under TEM, the MoS_2 nanoparticles of tens of nanometers in sizes with undefined shapes appeared highly conformed to the hG

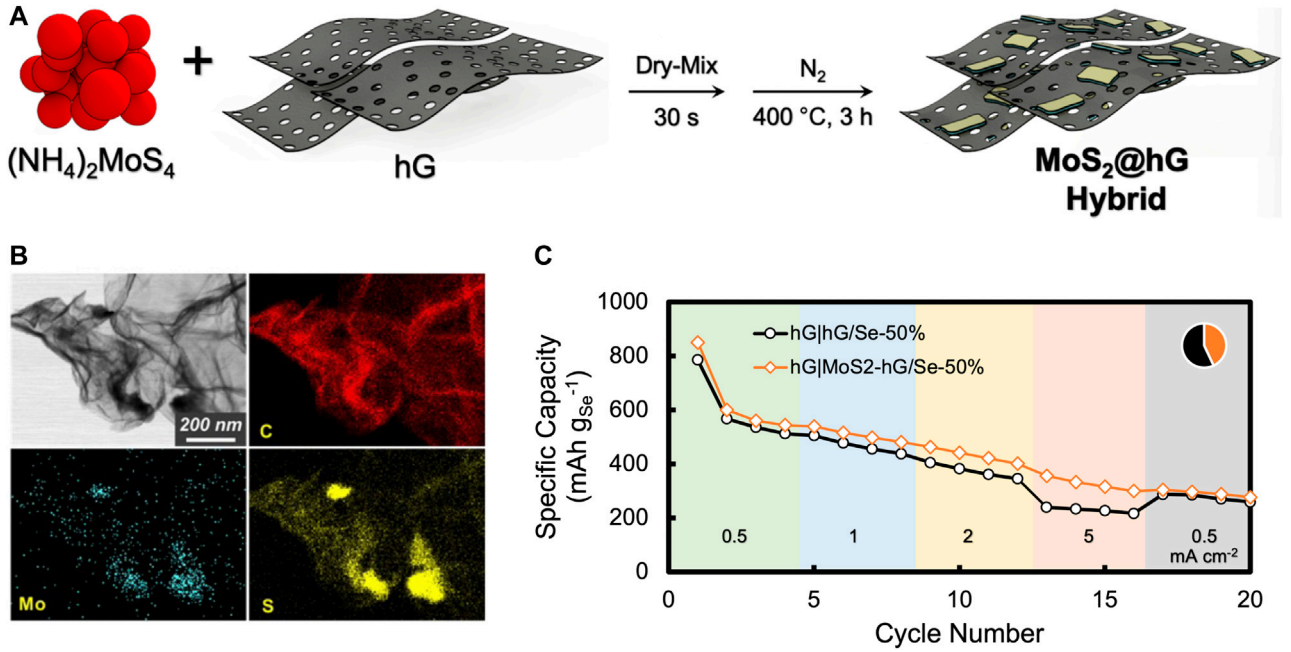

FIGURE 5 | Toward entrapping soluble polyselenides: **(A)** solvent-free synthesis of the MoS_2@hG hybrid; **(B)** a typical TEM image and the corresponding C, Mo, and S EDS maps of the MoS_2@hG hybrid; **(C)** Li-Se battery performance with a hG|hG/Se-50% cathode vs. a hG|MoS_2-hG/Se-50% cathode in a protocol, where J_A was sequentially held at 0.5, 1, 2, 5, 0.5 mA cm^{-2} (each for 4 cycles).

surface, likely due to their two-dimensional crystalline nature (**Figure 5B**).

With the entire process being solvent free, the resultant MoS_2@hG hybrid powder was mixed with neat hG in a 1:1 weight ratio to serve as a compressible host matrix for the Se active material. Robust composite MoS_2-hG/Se cathode discs were conveniently fabricated *via* the same mix-and-press approach. In a proof-of-concept experiment, Li-Se battery cells with a hG|hG/Se-50% cathode and a hG|MoS_2-hG/Se-50% [i.e., (MoS_2@hG:hG):Se = (1:1):2, w/w] cathode were fabricated. The total cathode mass loadings were both 32.9 mg cm^{-2}, which include the 2.9 mg cm^{-2} hG interlayer. The Se mass loadings in both cells were 8.6 mg cm^{-2}. As shown in **Figure 5C**, the incorporation of MoS_2 into the cathode improved the capacity retention at various current densities, with the step-like cycling protocol in the early cycles. For example, the capacities were 421 vs. 362 mAh g_{Se}^{-1} at cycle 11 (J_A = 2 mA cm^{-2}) and 316 vs. 227 mAh g_{Se}^{-1} at cycle 15 (J_A = 5 mA cm^{-2}), respectively. However, the improvement effect diminished after about 20 cycles, with the overall capacity loss remaining significant (>80% after 40 cycles). A likely scenario is that the available MoS_2 became saturated with the adsorbed polyselenides and gradually deactivated due to ultrahigh Se mass loading. Such a phenomenon has not been much discussed in the literature because most of the reported work in this area used low cathode mass loadings, and, therefore, the adsorbent capacity was likely not reached (Liu et al., 2017; Rana et al., 2020; Ye and Lee, 2020).

Nevertheless, these preliminary results still suggest that such a hybrid incorporation strategy can be viable for more effectively entrapping soluble polyselenides, and further optimization of the composition and content of the entrapment species is required. These methods, along with other polyselenide mitigation strategies such as separator coatings, electrolytes with low intermediate solubility and solid-state electrolytes, will be explored in future studies.

CONCLUSION

A facile mix-and-press electrode fabrication technique is demonstrated to prepare dense and ultrahigh Se mass loading cathodes without the need of solvents or a binder. The technique is enabled by using hG as a conductive and architectural scaffold. Up to 90 wt% Se content and 15.6 mg cm^{-2} Se mass loading in the cathodes are demonstrated, with high Se utilizations (>85%) and a remarkable initial areal capacity of 9 mAh cm^{-2}. The unique dry-press electrode fabrication also allows for the preparation of a layered electrode architecture, where a lightweight, neat hG layer is inserted between the current collector and the active material composite layer to improve the electrical contact. It is also demonstrated that polyselenide entrapment species, such as MoS_2, may be incorporated with the hG scaffold and subsequently into the ultrahigh Se mass loading cathodes to improve capacity retention and compatibility with the solvent-free mix-and-press approach. There was still significant shuttling of polyselenides despite the performance improvements in initial cycles. Further studies are underway

to incorporate more effective polyselenide mitigation strategies to improve the long-term cycling performance of these ultrahigh Se mass loading Li-Se batteries.

DATA AVAILABILITY STATEMENT

The original contributions presented in the study are included in the article/**Supplementary Material**; further inquiries can be directed to the corresponding authors.

AUTHOR CONTRIBUTIONS

Experiments and concepts were designed by YL and JC. Data collection and analysis was conducted by CP-R and YL. Original draft was written by CP-R and YL. Data interpretation and manuscript review/edit were conducted by all authors: CP-R, RV, DD, JW, JC, and YL.

FUNDING

Financial support from the NASA Convergent Aeronautics Solutions (CAS) program is gratefully acknowledged. C. Plaza-Rivera was a NASA Interns, Fellows, and Scholars (NIFS) Program intern supported by CAS.

ACKNOWLEDGMENTS

We thank J. Baughman, J.-W. Kim, and G. Sauti for experimental assistance.

SUPPLEMENTARY MATERIAL

The Supplementary Material for this article can be found online at: https://www.frontiersin.org/articles/10.3389/fenrg.2021.703676/full#supplementary-material

REFERENCES

Abouimrane, A., Dambournet, D., Chapman, K. W., Chupas, P. J., Weng, W., and Amine, K. (2012). A New Class of Lithium and Sodium Rechargeable Batteries Based on Selenium and Selenium-Sulfur as a Positive Electrode. *J. Am. Chem. Soc.* 134, 4505–4508. doi:10.1021/ja211766q

Bhargav, A., He, J., Gupta, A., and Manthiram, A. (2020). Lithium-sulfur Batteries: Attaining the Critical Metrics. *Joule* 4, 285–291. doi:10.1016/j.joule.2020.01.001

Chung, S.-H., Chang, C.-H., and Manthiram, A. (2018). Progress on the Critical Parameters for Lithium-Sulfur Batteries to Be Practically Viable. *Adv. Funct. Mater.* 28, 1801188. doi:10.1002/adfm.201801188

Eftekhari, A. (2017). The Rise of Lithium-Selenium Batteries. *Sust. Energ. Fuels* 1, 14–29. doi:10.1039/c6se00094k

Gu, X., and Lai, C. (2019). One Dimensional Nanostructures Contribute Better Li-S and Li-Se Batteries: Progress, Challenges and Perspectives. *Energ. Storage Mater.* 23, 190–224. doi:10.1016/j.ensm.2019.05.013

Gu, X., Tang, T., Liu, X., and Hou, Y. (2019). Rechargeable Metal Batteries Based on Selenium Cathodes: Progress, Challenges and Perspectives. *J. Mater. Chem. A.* 7, 11566–11583. doi:10.1039/c8ta12537f

Han, X., Yang, Z., Zhao, B., Zhu, S., Zhou, L., Dai, J., et al. (2017). Compressible, Dense, Three-Dimensional Holey Graphene Monolithic Architecture. *ACS Nano* 11, 3189–3197. doi:10.1021/acsnano.7b00227

Hawley, W. B., and Li, J. (2019). Electrode Manufacturing for Lithium-Ion Batteries-Analysis of Current and Next Generation Processing. *J. Energ. Storage* 25, 100862. doi:10.1016/j.est.2019.100862

Huang, L., Li, J., Liu, B., Li, Y., Shen, S., Deng, S., et al. (2020). Electrode Design for Lithium-Sulfur Batteries: Problems and Solutions. *Adv. Funct. Mater.* 30, 1910375. doi:10.1002/adfm.201910375

Kirsch, D. J., Lacey, S. D., Kuang, Y., Pastel, G., Xie, H., Connell, J. W., et al. (2019). Scalable Dry Processing of Binder-free Lithium-Ion Battery Electrodes Enabled by Holey Graphene. *ACS Appl. Energ. Mater.* 2, 2990–2997. doi:10.1021/acsaem.9b00066

Kraytsberg, A., and Ein-Eli, Y. (2016). Conveying Advanced Li-Ion Battery Materials into Practice the Impact of Electrode Slurry Preparation Skills. *Adv. Energ. Mater.* 6, 1600655. doi:10.1002/aenm.201600655

Kumar, R., Liu, J., Hwang, J.-Y., and Sun, Y.-K. (2018). Recent Research Trends in Li-S Batteries. *J. Mater. Chem. A.* 6, 11582–11605. doi:10.1039/c8ta01483c

Lin, Y., Han, X., Campbell, C. J., Kim, J.-W., Zhao, B., Luo, W., et al. (2015). Holey Graphene Nanomanufacturing: Structure, Composition, and Electrochemical Properties. *Adv. Funct. Mater.* 25, 2920–2927. doi:10.1002/adfm.201500321

Lin, Y., Jones, K. J., Greenburg, L. C., Kim, J. W., Hu, L., and Connell, J. W. (2019). Facile, Solvent-Free Preparation of High Density, High Mass Loading Sulfur Cathodes Enabled by Dry-Pressable Holey Graphene Scaffolds. *Batteries. Supercaps.* 2, 774–783. doi:10.1002/batt.201900053

Lin, Y., Moitoso, B., Martinez-Martinez, C., Walsh, E. D., Lacey, S. D., Kim, J.-W., et al. (2017). Ultrahigh-capacity Lithium-Oxygen Batteries Enabled by Dry-Pressed Holey Graphene Air Cathodes. *Nano Lett.* 17, 3252–3260. doi:10.1021/acs.nanolett.7b00872

Lin, Y., Watson, K. A., Fallbach, M. J., Ghose, S., Smith, J. G., Delozier, D. M., et al. (2009). Rapid, Solventless, Bulk Preparation of Metal Nanoparticle-Decorated Carbon Nanotubes. *ACS Nano* 3, 871–884. doi:10.1021/nn8009097

Liu, T., Jia, M., Zhang, Y., Han, J., Li, Y., Bao, S., et al. (2017b). Confined Selenium within Metal-Organic Frameworks Derived Porous Carbon Microcubes as Cathode for Rechargeable Lithium-Selenium Batteries. *J. Power Sourc.* 341, 53–59. doi:10.1016/j.jpowsour.2016.11.099

Liu, X., Huang, J.-Q., Zhang, Q., and Mai, L. (2017a). Nanostructured Metal Oxides and Sulfides for Lithium-Sulfur Batteries. *Adv. Mater.* 29, 1601759. doi:10.1002/adma.201601759

Manthiram, A. (2020). A Reflection on Lithium-Ion Battery Cathode Chemistry. *Nat. Commun.* 11, 1550. doi:10.1038/s41467-020-15355-0

Plaza-Rivera, C. O., Walker, B. A., Tran, N. X., Viggiano, R. P., Dornbusch, D. A., Wu, J. J., et al. (2020). Dry Pressing Neat Active Materials into Ultrahigh Mass Loading sandwich Cathodes Enabled by Holey Graphene Scaffold. *ACS Appl. Energ. Mater.* 3, 6374–6382. doi:10.1021/acsaem.0c00582

Pope, M. A., and Aksay, I. A. (2015). Structural Design of Cathodes for Li-S Batteries. *Adv. Energ. Mater.* 5, 1500124. doi:10.1002/aenm.201500124

Rana, M., Luo, B., Kaiser, M. R., Gentle, I., and Knibbe, R. (2020). The Role of Functional Materials to Produce High Areal Capacity Lithium Sulfur Battery. *J. Energ. Chem.* 42, 195–209. doi:10.1016/j.jechem.2019.06.015

Sun, J., Du, Z., Liu, Y., Ai, W., Wang, K., Wang, T., et al. (2021). State-Of-The-Art and Future Challenges in High Energy Lithium-Selenium Batteries. *Adv. Mater.* 33, 2003845. doi:10.1002/adma.202003845

Walker, B. A., Plaza-Rivera, C. O., Sun, S.-S., Lu, W., Connell, J. W., and Lin, Y. (2020). Dry-pressed Lithium Nickel Cobalt Manganese Oxide (NCM) Cathodes Enabled by Holey Graphene Host. *Electrochimica Acta* 362, 137129. doi:10.1016/j.electacta.2020.137129

Walsh, E. D., Han, X., Lacey, S. D., Kim, J.-W., Connell, J. W., Hu, L., et al. (2016). Dry-processed, Binder-free Holey Graphene Electrodes for Supercapacitors with Ultrahigh Areal Loadings. *ACS Appl. Mater. Inter.* 8, 29478–29485. doi:10.1021/acsami.6b09951

Wenzel, V., Nirschl, H., and Nötzel, D. (2015). Challenges in Lithium-Ion-Battery Slurry Preparation and Potential of Modifying Electrode Structures by Different Mixing Processes. *Energ. Tech.* 3, 692–698. doi:10.1002/ente.201402218

Xu, G.-L., Liu, J., Amine, R., Chen, Z., and Amine, K. (2017). Selenium and Selenium-Sulfur Chemistry for Rechargeable Lithium Batteries: Interplay of Cathode Structures, Electrolytes, and Interfaces. *ACS Energ. Lett.* 2, 605–614. doi:10.1021/acsenergylett.6b00642

Ye, H., and Lee, J. Y. (2020). Solid Additives for Improving the Performance of Sulfur Cathodes in Lithium-Sulfur Batteries-Adsorbents, Mediators, and Catalysts. *Small Methods* 4, 1900864. doi:10.1002/smtd.201900864

Zhao, M., Li, B.-Q., Zhang, X.-Q., Huang, J.-Q., and Zhang, Q. (2020). A Perspective toward Practical Lithium-Sulfur Batteries. *ACS Cent. Sci.* 6, 1095–1104. doi:10.1021/acscentsci.0c00449

Conflict of Interest: The authors declare that the research was conducted in the absence of any commercial or financial relationships that could be construed as a potential conflict of interest.